SCIENTIFIC REPORTS

OPEN

SUBJECT AREAS:
IMAGING AND SENSING
MAGNETO-OPTICS

Received
22 January 2014

Accepted
15 April 2014

Published
16 July 2014

Correspondence and requests for materials should be addressed to A.M.Z. (zheltikov@physics.msu.ru)

Electron spin manipulation and readout through an optical fiber

I. V. Fedotov[1,2], L. V. Doronina-Amitonova[1,2,3], A. A. Voronin[1,2], A. O. Levchenko[4], S. A. Zibrov[4], D. A. Sidorov-Biryukov[1,2], A. B. Fedotov[1,2], V. L. Velichansky[4] & A. M. Zheltikov[1,2,5]

[1]Physics Department, International Laser Center, M.V. Lomonosov Moscow State University, Moscow 119992, Russia, [2]Russian Quantum Center, ul. Novaya 100, Skolkovo, Moscow Region, 1430125 Russia, [3]Department of Neuroscience, Kurchatov Institute National Research Center, Moscow, Russia, [4]P.N. Lebedev Physical Institute, Russian Academy of Sciences, Leninsky pr. 53, Moscow 119991, Russia, [5]Department of Physics and Astronomy, Texas A&M University, College Station TX 77843, USA.

The electron spin of nitrogen--vacancy (NV) centers in diamond offers a solid-state quantum bit and enables high-precision magnetic-field sensing on the nanoscale. Implementation of these approaches in a fiber format would offer unique opportunities for a broad range of technologies ranging from quantum information to neuroscience and bioimaging. Here, we demonstrate an ultracompact fiber-optic probe where a diamond microcrystal with a well-defined orientation of spin quantization NV axes is attached to the fiber tip, allowing the electron spins of NV centers to be manipulated, polarized, and read out through a fiber-optic waveguide integrated with a two-wire microwave transmission line. The microwave field transmitted through this line is used to manipulate the orientation of electron spins in NV centers through the electron-spin resonance tuned by an external magnetic field. The electron spin is then optically initialized and read out, with the initializing laser radiation and the photoluminescence spin-readout return from NV centers delivered by the same optical fiber.

Due to their remarkable electron-spin properties, nitrogen–vacancy (NV) centers in diamond offer a unique solid-state system for quantum science and technologies[1–4]. The electron spin of NV centers in diamond display an extraordinarily long-lived coherence even at room temperatures[1,5], enabling coherence-control-enhanced quantum data processing[2,3]. NV centers have been shown to allow the creation of efficient and stable solid-state single-photon sources and to offer unprecedented opportunities for bioimaging[6,7], highly sensitive nanoscale magnetometry[8–10], thermometry of single living cells[11], as well as high spatial and temporal resolution imaging of neural activity[12].

Many of the emerging unique NV-diamond-based technologies call for suitable fiber solutions that would open the ways toward the development of a new class of quantum information devices and sensors for a broad range of applications, including high-precision magnetometry, bioimaging, neurosciences and medical diagnostics. To achieve this goal, however, several challenging issues have to be addressed. First, technologies allowing NV centers to be coupled with optical fibers need to be developed. Second, fiber-optic delivery of the readout laser radiation has to be combined with fiber-optic collection of fluorescence from NV centers and fiber-optic transmission of this fluorescence signal to an optical detection system. Finally, the bidirectional fiber-optic delivery of the readout field and the fluorescence response needs to be integrated with efficient transmission of microwave radiation to the tip of the fiber probe.

Here, we demonstrate an ultracompact fiber-optic platform that offers solutions to all the above-listed problems, allowing the electron spin of NV centers in diamond deposited in the tip of an optical fiber to be manipulated, polarized, and read out using the fiber-optic delivery of optical radiation integrated with a specially designed transmission line for microwave fields. The microwave field transmitted through this line, running along the optical fiber, induces the electron spin resonance (ESR) in the spin-triplet ground state of NV centers in diamond deposited on the fiber tip. The ESR, tuned by an external magnetic field, is read out, through the optical fiber, via the spin-dependent photoluminescence (PL) of NV centers excited by visible laser radiation, delivered by the same optical fiber.

Our experiments were performed using NV centers in diamond crystals approximately 250 μm in diameter, attached to the tip of a multimode optical fiber (Fig. 1a). While the earlier studies have demonstrated the possibility of embedding diamond nanoparticles into specially designed, photonic-crystal[13,14] and tapered[15] optical fibers, in this work, microcrystals of diamond, irradiated with MeV electrons and annealed

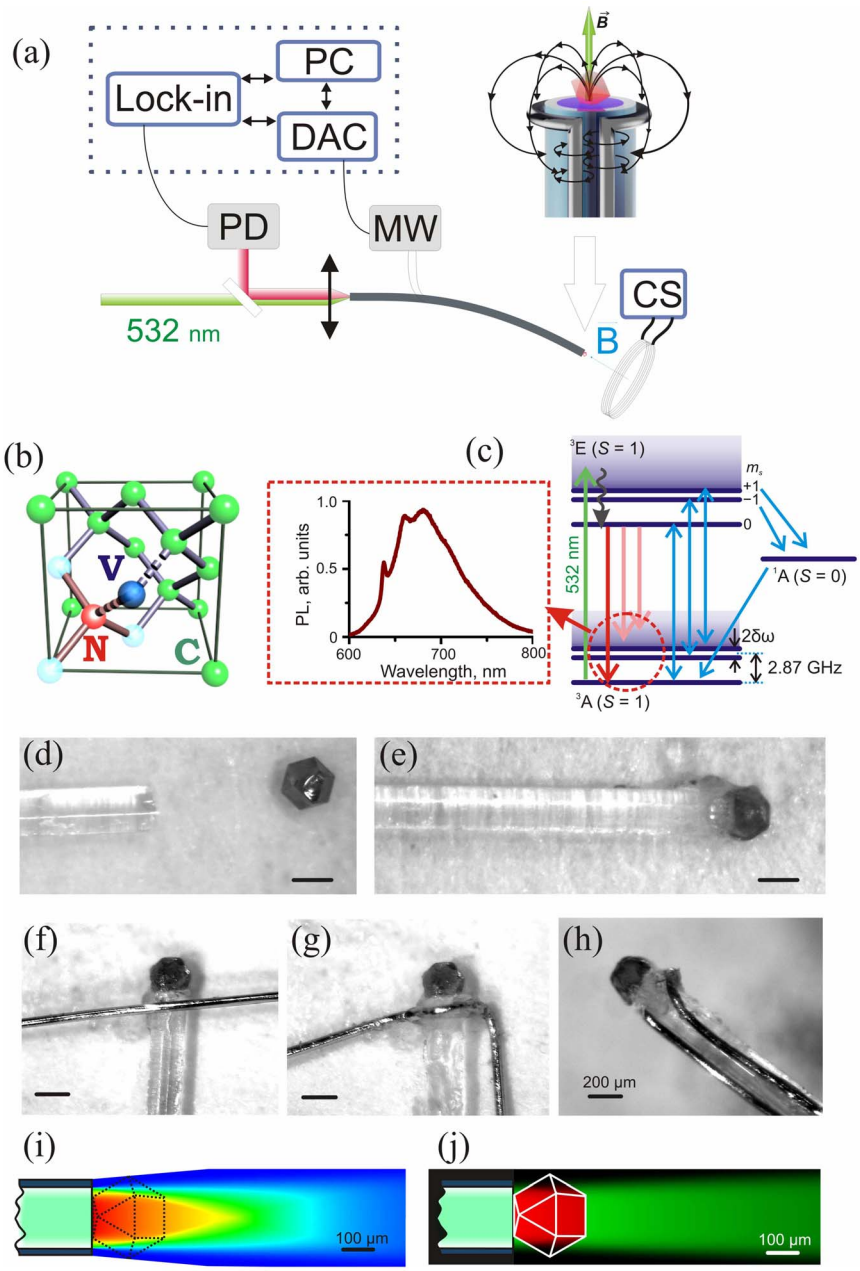

Figure 1 | Electron spin manipulation, polarization, and readout through an optical fiber. (a) Diagram of the experimental setup: PD, photodiode; MW, microwave source; CS, source of dc current; PC, computer; DAC, digital-to-analog converter; Lock-in, lock-in amplifier; L, lens. The inset sketches an optical fiber integrated with a short-circuited two-wire microwave transmission line and with a diamond microcrystal attached to its tip. Also shown are the lines of the microwave field induced by the wires and the loop short-circuiting the transmission line. (b) A nitrogen atom (N) and a vacancy (V) forming an NV center in a diamond lattice, consisting of carbon (C) atoms. Four possible arrangements of the NV axis with respect to the crystal lattice of diamond are shown. (c) Diagram of energy levels involved in electron-spin spectroscopy. The ground state of NV centers in diamond is a spin-triplet state with a zero-field splitting $\Omega_s \approx 2.87$ GHz. When tuned to the ESR frequency Ω_s, a microwave field efficiently transfers population from the $m_s = 0$ to the $m_s = \pm 1$ state. An optical pump at 532 nm couples the ^3A ground electronic state to the ^3E excited state, giving rise to photoluminescence, shown by the red line, featuring a characteristic zero-phonon line at approximately 637 nm, which is observed in the spectrum of photoluminescence (shown on the left) against a broad phonon-sideband line, stretching down to 800 nm. An external magnetic field removes the degeneracy of the $m_s = \pm 1$ state and induces a Zeeman frequency shift $2\delta\omega$ between these sublevels. A substantial fraction of the $m_s = \pm 1$ excited-state population is transferred to the $m_s = 0$ ground level via a metastable ^1A singlet state. (d–h) Steps 1–5 of fiber-probe fabrication, as described in the Methods section. The scale bar is 200 μm. (i, j) The maps of the $\psi(r, z)$ function (i) and the PL spin-readout return function $H(r, z)\psi(r, z)$ (j) for the fiber-optic probe used in the experiments.

to a typical density of NV centers on the order of 10^{14} cm^{-3}, were attached to the tip of an optical fiber for enhanced coupling of the fluorescence spin readout to the guided modes of the fiber probe.

The spin part of the electron Hamiltonian of an NV center in the presence of an external magnetic field **B** is written as[8,9,16]

$$H = \mu_B g \mathbf{BS} + D\left[S_Z^2 - \frac{S(S+1)}{3}\right] + E\left(S_X^2 - S_Y^2\right), \qquad (1)$$

where μ_B is the Bohr magneton, $g \approx 2$ is the electron g-ratio, D and E are the zero-magnetic-field splitting parameters, S_j ($j = X, Y, Z$) are

the projections of the electron spin **S** on the principal Cartesian coordinate axes *X*, *Y*, *Z*, with the *Z*-axis chosen along the N--V axis (Fig. 1b). The first term in Eq. (1) describes the Zeeman effect in an external magnetic field, which is observed against zero-field splitting due to the crystal field, governed by the second and third terms in Eq. (1), dominated by the splitting $\Omega_s = D/h \approx 2.87$ GHz (h being the Planck constant) between the $m_s = 0$ spin state and the twofold-degenerate $m_s = \pm 1$ state (Fig. 1c).

The electron spin of the ground-state triplet of NV centers is manipulated by a microwave field through the ESR. The microwave field is delivered to the diamond microcrystal with NV centers through a two-wire transmission line, running along the optical fiber (the inset to Fig. 1a) and consisting of a pair of copper wires 50 μm in diameter each. The procedure used to integrate a fiber-optic probe with a microwave transmission line and an NV-diamond microcrystal (Figs. 1d–1h) is described in the Methods section below. The two-wire transmission line is short-circuited with a loop, winding around the fiber tip (the inset to Fig. 1a) and inducing a microwave field distribution with a maximum at the location of diamond microcrystal. When tuned to the ESR frequency Ω_s, this microwave field efficiently transfers population from the $m_s = 0$ to the $m_s = \pm 1$ state (Fig. 1c), thus manipulating spin orientation.

Optical initialization of NV centers in diamond is provided by the 50-mW, 532-nm second-harmonic output of a continuous-wave Nd:YAG laser, which is delivered to the diamond microcrystal attached to the tip of the fiber, along the 200-μm-diameter core of the fiber probe (Fig. 1a). This laser radiation couples the ^3A ground electronic state to the ^3E excited state, giving rise to photoluminescence (the red line in Fig. 1c), featuring a characteristic zero-phonon line, which is observed at approximately 637 nm at room temperature against a broad phonon-sideband line, stretching down to 800 nm (Fig. 1c, left). The photoluminescence emitted by laser-initialized NV centers within the 630–800-nm wavelength range is collected by the same optical fiber, providing a high efficiency of photoluminescence collection (see Fig. 1i and the Methods section) due to its high numerical aperture (NA = 0.22), and is transmitted through this fiber to the detection system, consisting of a silicon photodiode, a low-noise preamplifier, and a lock-in amplifier (Fig. 1a).

For NV centers in the $m_s = \pm 1$ state, the photoluminescence yield is lower than that typical of NV centers in the $m_s = 0$ state, because a substantial fraction of the $m_s = \pm 1$ excited-state population is transferred to the $m_s = 0$ ground level via a metastable singlet state (the ^1A state in Fig. 1c). This pathway does not contribute to the 630–800-nm photoluminescence band, allowing optical detection of ESR with the spin state read out from the intensity of the photoluminescence signal. An external magnetic field **B** removes the degeneracy of the $m_s = \pm 1$ state and induces a Zeeman frequency splitting $\Delta\Omega_Z$ between the $m_s = \pm 1$ sublevels (Fig. 1c). Since the photoluminescence from $m_s = \pm 1$ levels is weaker than the photoluminescence from $m_s = 0$ states, the Zeeman-shifted sublevels are observed as **B**-dependent features in the intensity of photoluminescence I_{PL} measured as a function of the microwave frequency Ω (Fig. 2a).

The C_{3v} symmetry of the crystal lattice of diamond dictates four possible orientations of the spin quantization axes (shown by axes 1, 2, 3, and 4 in Fig. 2b) relative to the crystal lattice. The plane defined by one pair of these axes (axes 1 and 2 in Fig. 2b), oriented at an angle $\varepsilon \approx 109.4^\circ$ with respect to each other, is perpendicular to the plane of the other two axes (axes 3 and 4 in Fig. 2b), which make the same angle $\varepsilon \approx 109.4^\circ$ with each other. Since four orientations of NV axes in the diamond lattice define four polar angles θ_i (i = 1, 2, 3, 4) between an external magnetic field **B** and each of the NV axes, it is convenient to describe **B** in a Cartesian system of coordinates where the *x*-, *y*-, and *z*-axes are introduced in such a way (Fig. 2b) that two of the four spin quantization axes (axes 1 and 2) lie in the *xy*-plane, the *z*-axis is perpendicular to this plane, and the *y*-axis is chosen along the bisector of the angle between the other two spin quantization axes (axes 3 and 4 in Fig. 2b) and belongs to the plane defined by these quantization axes.

The polar angle θ of a magnetic field **B** relative to the z-axis of this system of coordinates and the azimuthal angle φ of this field measured in the *xy*-plane (Figs. 2b, 3b) can be then expressed through the polar angles θ_i between **B** and the four NV axes (i = 1, 2, 3, 4) in the diamond lattice as $\cos\theta_1 = \sin\theta\sin(\varepsilon/2 - \varphi)$, $\cos\theta_2 = -\sin\theta\sin(\varepsilon/2 + \varphi)$, $\cos\theta_3 = \cos(\varepsilon/2)\sin\theta\sin\varphi + \sin(\varepsilon/2)\cos\theta$, and $\cos\theta_4 = \cos(\varepsilon/2)\sin\theta\sin\varphi - \sin(\varepsilon/2)\cos\theta$, with the angles θ_i meeting an obvious identity $\sum_{i=1}^{4} \cos\theta_i = 0$.

The characteristic equation for the spin Hamiltonian (1) with $E \ll D$ yields the following solutions[10] for the magnitude of the magnetic field, B, and each of the polar angles θ_i:

$$B^2 = \frac{1}{3\mu_B^2 g^2}\left(\Omega_{1i}^2 + \Omega_{2i}^2 - \Omega_{1i}\Omega_{2i} - D^2\right) - E^2, \qquad (2)$$

$$\cos(2\theta_i) \approx \frac{7D^3 + 2(\Omega_{1i} + \Omega_{2i})\left[2\left(\Omega_{1i}^2 + \Omega_{2i}^2\right) - 5\Omega_{1i}\Omega_{2i} - 9E^2\right] - 3D\left(\Omega_{1i}^2 + \Omega_{2i}^2 - \Omega_{1i}\Omega_{2i} + 9E^2\right)}{9D\left(\Omega_{1i}^2 + \Omega_{2i}^2 - \Omega_{1i}\Omega_{2i} - D^2 - 3E^2\right)}, \qquad (3)$$

where Ω_{1i} and Ω_{2i} are the frequencies of the Zeeman-split ESR peaks in $I_{PL}(\Omega)$ spectra corresponding to four (i = 1, 2, 3, 4) orientations of the NV axis in the diamond lattice.

It is straightforward to see from Eq. (2) that, once the $I_{PL}(\Omega)$ spectrum in the absence of an external magnetic field has been measured, the magnitude of the magnetic field can be reliably determined from the best fit of $I_{PL}(\Omega)$ spectra measured in the presence of an external magnetic field. Since the positions of four Zeeman peaks have to be simultaneously fitted using B as a single fitting parameter (Fig. 2c), this procedure enables a high-fidelity determination of B. Finding the orientation of **B** is, however, less straightforward. Since the four NV axes are physically indistinguishable, an auxiliary bias magnetic field of known orientation would be generally needed to determine the absolute orientation of **B**.

With a diamond microcrystal fixed on the tip of an optical fiber, the orientation of the spin quantization axes needs to be determined relative to the fiber axis. To this end, the intensity I_{PL} of the spin-dependent photoluminescence from NV centers was measured as a function of the frequency Ω of the microwave field used to modulate the ESR in the presence of an external magnetic field **B** directed along the fiber axis (Fig. 2b), with the polar and azimuthal angles of the fiber axis relative to the crystallographic *z*-axis being equal to $\theta_f = \theta$ and $\varphi_f = \varphi$. As can be seen from Fig. 2a, the $I_{PL}(\Omega)$ dependences measured through the optical fiber with a diamond microcrystal attached to its tip exhibit four well-resolved peaks on either side of the central ESR frequency $\Omega_s \approx 2.87$ GHz. Each of these peaks represents a projection of the external magnetic field on one of the four spin quantization axes, with its frequency shift increasing with B, as shown in Fig. 2c. With each Zeeman-shifted peak approximated with a Gaussian spectral profile, the best fit for the frequency shifts of all the four peaks measured as functions of the magnitude of the external magnetic field is achieved (solid lines in Figs. 2a and 2c) with $\theta_f = \theta \approx 24^\circ$ and $\varphi_f = \varphi \approx -56^\circ$.

With the orientation of spin quantization axes defined, the magnitude of an external magnetic field **B** with unknown orientation and variations in its orientation can be measured with a high accuracy from the shifts of the Zeeman peaks in the $I_{PL}(\Omega)$ spectrum. Figure 3a presents the results of experiments performed with an external magnetic field lying in the *xz*-plane and making an angle $\theta \approx 8^\circ$ with the *z*-axis of our crystallographic system of coordinates (Fig. 3b). A magnetic field with such an orientation has two pairs of equal components along the NV axes – one pair of components along NV axes 1 and 2 and the other pair along the axes 3 and 4. With such an orientation of the external magnetic field, the number of nonequal field projections on the NV axes is reduced, and the photoluminescence intensity measured as a function of the microwave frequency

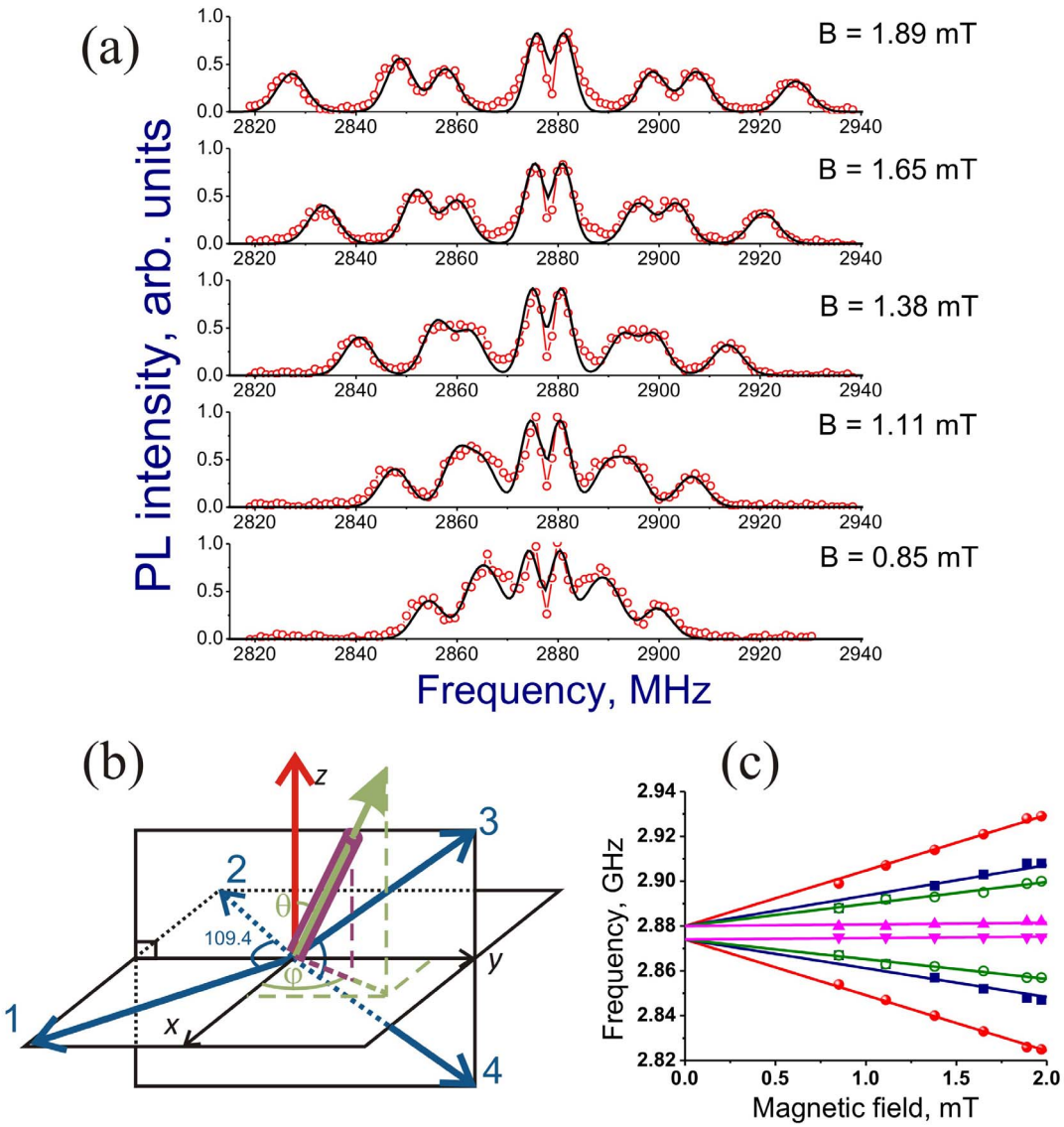

Figure 2 | (a) Intensity of photoluminescence from NV centers as a function of the frequency of the microwave field inducing the electron spin resonance in the presence of a variable magnetic field **B** applied along the axis of the optical fiber. (b) Orientation of the fiber axis and the magnetic field (green line) and four N–V axes (axes 1–4). The *x*-, *y*-, and *z*-coordinate axes are related to the crystal lattice with NV axes 1 and 2 lying in the *xy*-plane, the *z*-axis perpendicular to this plane, and the *y*-axis chosen along the bisector of the angle between NV axes 3 and 4 and belonging to the plane defined by these axes. (c) The frequencies of the four pairs of the Zeeman-shifted peaks as functions of the magnitude of the magnetic field: (dots) experimental data and (solid lines) calculations using the model described in the text with *B* treated as a fitting parameter.

features only two pairs of Zeeman-shifted features on either side of the ESR frequency (Fig. 3a). The standard theory of Zeeman splitting applied to NV centers in diamond provides an accurate fit for the positions of all the peaks measured as functions of the magnitude of the external magnetic field (cf. the dots and solid lines in Fig. 3c), verifying the ability of the fiber-optic probe for magnetic field sensing.

To summarize, we have demonstrated an ultracompact fiber-optic probe where a diamond microcrystal with a well-defined orientation of spin quantization NV axes is attached to the fiber tip, allowing the electron spins of NV centers to be manipulated, polarized, and read out through a fiber-optic waveguide integrated with a two-wire microwave transmission line. The microwave field transmitted through this line is used to manipulate the orientation of electron spins in NV centers through the electron-spin resonance tuned by an external magnetic field. The electron spin is then optically initialized and read out, with the initializing laser radiation and the photoluminescence spin-readout return from NV centers delivered by the same optical fiber. The specific scheme of fiber-optic ESR spectroscopy demonstrated in this work is not designed for the highest sensitivity of magnetic field sensing, which can be achieved using, e.g., properly optimized optical and microwave spin-echo pulse sequences. However, it offers the key elements enabling ESR magnetometry, all integrated in the fiber format.

Methods

Fabrication of fiber-optic probes. The fiber-optic probes used in experiments were fabricated under a 4× microscope with a working distance of 25 cm following the procedure described below.

Step 1: Use an optical fiber with a core diameter of 200 μm and a cladding diameter of 220 μm. Remove protective polymer coating off the fiber. Use a ruby cutter for high-quality cuts on both ends of the fiber (Fig. 1d). The length of the fiber can be varied within a broad range, from a few centimeters to a few meters, depending on the experimental arrangement. Experiments presented here were performed with a 25-cm-long fiber probe.

Step 2: Use fine mechanical tweezers to place a diamond microcrystal on the tip of the fiber and fix it with a cyanoacrylate glue (Fig. 1e). Wait approximately an hour until the glue solidifies.

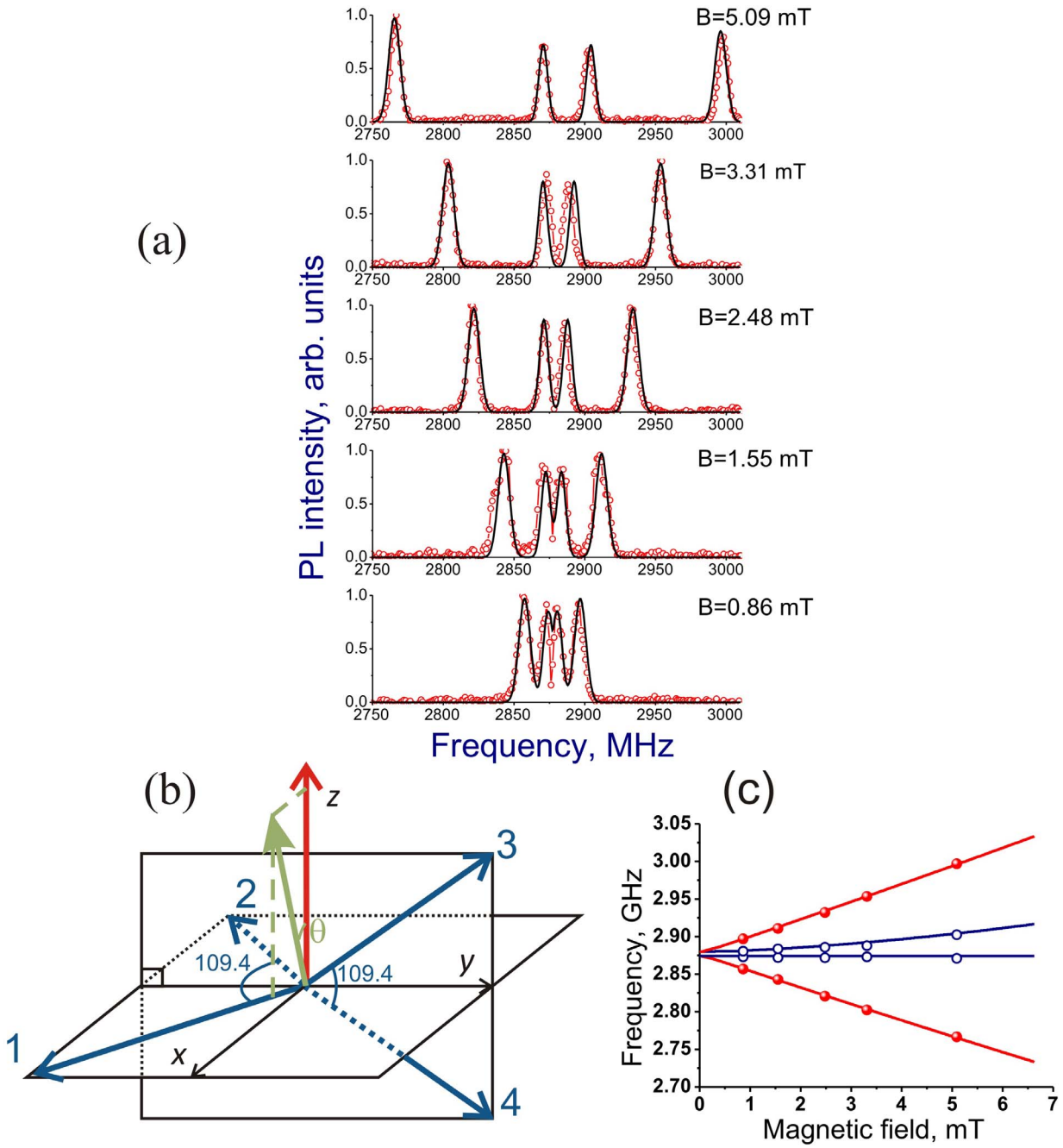

Figure 3 | (a) Intensity of photoluminescence from NV centers as a function of the frequency of the microwave field inducing the electron spin resonance in the presence of a variable magnetic field **B** oriented as shown in panel (b). (c) The frequencies of the two pairs of the Zeeman-shifted peaks as functions of the magnitude of the magnetic field: (dots) experimental data and (solid lines) calculations using the model described in the text with B treated as a fitting parameter.

Step 3: Position a 50-μm-diameter copper wire perpendicular to the fiber near the fiber tip, as shown in Fig. 1f, and fix the central part of the wire to the fiber with a cyanoacrylate glue. Wait approximately an hour until the glue solidifies.

Step 4: Use fine mechanical tweezers and/or a metal needle to bend the copper wire around the fiber (Fig. 1g).

Step 5: Use fine mechanical tweezers and/or a metal needle to bend the copper wire on either side of the fiber in such a way as to align the wire with the fiber (Figs. 1g, 1h). Adjust the length of the copper wire to match the required length of the fiber probe and to minimize impedance mismatch. Fix this wire arrangement with a cyanoacrylate glue. Wait approximately an hour until the glue solidifies.

Optical initialization and collection of the photoluminescence spin readout signal. Optical initialization of NV centers in diamond is provided by the 50-mW, 532-nm second-harmonic output of a continuous-wave Nd: YAG laser, which is delivered to the diamond microcrystal attached to the tip of the fiber, along the 200-μm-diameter core of the fiber probe (Fig. 1a). The photoluminescence emitted by laser-initialized NV centers within the 630–800-nm wavelength range is collected by the same optical fiber (Figs. 1a, 1i, 1j).

The ability of the fiber probe to collect the photoluminescence spin readout signal from NV centers is quantified in terms of the total power of the PL signal collected by the fiber probe, which is written as[17] $P \propto \sigma\eta N_0 I_0 \int_0^\infty dz \int_0^\infty H(r,z)\psi(r,z) r dr$, where σ is the absorption cross section, η is the PL quantum yield, N_0 and $H(r, z)$ are the maximum density and the spatial distribution of NV centers in the diamond microcrystal, r is the transverse coordinate measured from the axis of the fiber probe, z is the longitudinal coordinate measured from the output end of the fiber probe, I_0 is the intensity of laser radiation at the center of the beam at the output end of the fiber probe, i.e., at $r = 0$ and $z = 0$, $\psi(r, z) = \phi(r, z)f(r, z)T(r, z)$, $\phi(r, z)$ is the efficiency of PL signal collection by the fiber probe, $f(r, z)$ is the factor including the divergence of the laser beam, $T(r, z)$ is the attenuation factor due to the absorption and scattering of laser and PL radiation, respectively. The product $H(r, z)\psi(r, z)$ under the integral

quantifies the contribution of an infinitesimal volume inside a diamond microcrystal centered at r and z to the total PL return collected by the fiber probe.

For a fiber probe with a numerical aperture $NA = \left(n_1^2 - n_2^2\right)^{1/2}$, where n_1 and n_2 are the refractive indices of the fiber core and cladding, respectively, we find $\phi(r, z) \approx \{1 - [1 - (NA/n_0)^2]^{1/2}\}/2$, where n_0 is the refractive index of the ambient medium. Since attenuation is negligible for our experimental conditions, we set $T(r, z) = 1$. The NV centers are assumed to be uniformly distributed over the diamond microcrystal, with the $H(r, z)$ function taken to be equal to 1 inside diamond and 0 otherwise. Laser beam divergence at the output of the fiber probe is included through $f(r,z) = a_m^2(z \tan \theta_d + a_m)^{-2}$, where a_m is the effective fiber mode radius and θ_d is the divergence angle of the laser beam.

As can be seen from Fig. 1i, which shows the map of the $\psi(r, z)$ function, the NA ≈ 0.22 optical fiber used in our experiments, due to its large core diameter, provides an almost uniform illumination of the diamond microcrystal attached to its end, as the typical longitudinal scale of beam divergence is much larger than the size of the diamond microcrystal (shown by a dashed contour line in Fig. 1i). This translates into an almost uniform distribution of the PL return signal within the diamond microcrystal, as shown in Fig. 1j. The PL return signal collection efficiency, $\zeta \approx \{1 - \cos[\arcsin(NA)]\}/2$, provided by our NA ≈ 0.22 fiber probe is estimated as $\zeta \approx 0.01$. This is to be compared with the highest ζ values, $\zeta \approx 0.28$, attainable in an oil-immersion-free confocal-microscopy arrangement with extremely high-NA (NA ≈ 0.9) objectives.

Characterization of diamond microcrystals. Diamond microcrystal characterization prior to fiber experiments included the assessment of the density of NV centers in a microcrystal. To this end, a diamond microcrystal was illuminated by 532-nm second-harmonic output of a continuous-wave Nd: YAG laser. The laser beam was focused on the microcrystal using a microobjective. The beam waist size of laser radiation was adjusted to be about 1 mm in order to provide a uniform illumination of the diamond microcrystal. The PL response of NV centers was collected with an NA = 0.2 lens, yielding a ratio of the PL power from NV centers to the power of laser radiation on the order of 10^{-5}. With a typical absorption cross section $\sigma \approx 3 \cdot 10^{-17}$ cm^2 and quantum yield $\eta \approx 0.1$ of NV centers in a diamond microcrystal with a volume of $1.5 \cdot 10^{-5}$ cm^3, this translates into a density of NV centers on the order of 10^{14} cm^{-3}.

Microwave transmission line. A two-wire microwave transmission line used to deliver the microwave field to a diamond microcrystal on the tip of an optical fiber (the inset to Fig. 1a) consists of a pair of copper wires running on either side of the optical fiber. The diameter of each wire is $d \approx 50$ μm. The distance between the wires is $S \approx 130$ μm. The length of the transmission line was varied from 15 to 50 cm. For the 20-cm-long transmission line used for the measurements presented here, the characteristic impedance of the transmission line, $Z \propto (\varepsilon_m)^{-1/2}\mathrm{acosh}(S/d)$, where ε_m is the permittivity of the dielectric medium surrounding the wires, is estimated as $Z \approx 190$ Ohm. The transmission loss of this line is $\alpha_l \approx 0.47$ m^{-1}.

Microwave excitation of electron-spin resonance. The microwave field is delivered by a compact microwave source with a typical output power up to 2 mW (e.g., a MiniCircuits ZX95-3100-S+ voltage-controlled oscillator), generating a microwave current tunable within the range of frequencies from 2.3 to 3.1 GHz with a step of about 1 MHz. The frequency of the microwave output is modulated with the use of a digit-to-analog converter controlled by home-made dedicated software. In experiments presented in this paper, the modulation frequency was $f_m \approx 1.13$ kHz. The lower frequency of the microwave output was set at 2.3 GHz, while the upper frequency was scanned from 2.5 to 3.1 GHz. The microwave output was coupled to the two-wire microwave transmission line, integrated into the fiber-optic probe, through a standard microwave coaxial cable and an SMA connector, soldered to the copper wire of the transmission line.

Detection of the photoluminescence spin readout. The photoluminescence spin readout signal from NV centers in a diamond microcrystal attached to the tip of the optical fiber is captured by the fiber probe and delivered to a detection system consisting of a silicon photodiode, a low-noise preamplifier, and a lock-in amplifier (Fig. 1a). As the upper frequency of the modulated microwave output is tuned to the ESR frequency Ω_e, the photoluminescence signal starts to oscillate at the frequency f_m, allowing lock-in amplification of the detected signal. To this end, the signal from the silicon photodiode is preprocessed with a low-noise preamplifier, allowing noise reduction, and detected with a lock-in amplifier at the frequency f_m. The residual noise of this detection system translates into an error in Zeeman peak frequency measurements (Figs. 2b, 2c, 3b, 3c) of 10–200 kHz, depending on the type of photodiode and amplification regime.

1. Gaebel, T. *et al.* Room-temperature coherent coupling of single spins in diamond. *Nat. Phys.* **2**, 408–413 (2006).
2. Dutt, M. G. *et al.* Quantum register based on individual electronic and nuclear spin qubits in diamond. *Science* **316**, 1312–1316 (2007).
3. Aharonovich, I., Greentree, A. D. & Prawer, S. Diamond photonics. *Nat. Photonics* **5**, 397–405 (2011).
4. Nizovtsev, A. P. *et al.* A quantum computer based on NV centers in diamond: Optically detected nutations of single electron and nuclear spins. *Opt. Spectrosc.* **99**, 233–244 (2005).
5. Childress, L. *et al.* Coherent Dynamics of Coupled Electron and Nuclear Spin Qubits in Diamond. *Science* **314**, 281–285 (2006).
6. McGuinness, L. P. *et al.* Quantum measurement and orientation tracking of fluorescent nanodiamonds inside living cells. *Nat. Nanotechnol.* **6**, 358–363 (2011).
7. Le Sage, D. *et al.* Optical magnetic imaging of living cells. *Nature* **496**, 486–489 (2013).
8. Taylor, J. M. *et al.* High-sensitivity diamond magnetometer with nanoscale resolution. *Nat. Phys.* **4**, 810–816 (2008).
9. Maze, J. R. *et al.* Nanoscale magnetic sensing with an individual electronic spin in diamond. *Nature* **455**, 644–647 (2008).
10. Balasubramanian, G. *et al.* Nanoscale imaging magnetometry with diamond spins under ambient conditions. *Nature* **455**, 648–651 (2008).
11. Kucsko, G. *et al.* Nanometre-scale thermometry in a living cell. *Nature* **500**, 54–58 (2013).
12. Hall, L. T. *et al.* High spatial and temporal resolution wide-field imaging of neuron activity using quantum NV-diamond. *Sci. Rep.* **2** (2012).
13. Schröder, T., Schell, A. W., Kewes, G., Aichele, T. & Benson, O. Fiber-integrated diamond-based single photon source. *Nano Lett.* **11**, 198–202 (2010).
14. Fedotov, I. V. *et al.* Guided-wave-coupled nitrogen vacancies in nanodiamond-doped photonic-crystal fibers. *Appl. Phys. Lett.* **101**, 031106–031106 (2012).
15. Liu, X. *et al.* Fiber-integrated diamond-based magnetometer. *Appl. Phys. Lett.* **103**, 143105 (2013).
16. Steinert, S. *et al.* Magnetic spin imaging under ambient conditions with sub-cellular resolution. *Nat. Commun.* **4**, 1607 (2013).
17. Doronina-Amitonova, L. V. *et al.* Enhancing the locality of optical interrogation with photonic-crystal fibers. *Appl. Phys. Lett.* **101**, 021114 (2012).

Acknowledgments

This research was supported in part by the Russian Foundation for Basic Research (projects nos. 13-02-01465, 13-02-92115, 14-02-90030) and the Welch Foundation (grant no. A-1801). Development of an optical fiber probe integrated with a microwave transmission line has been supported by the Russian Science Foundation (project no.14-12-00772).

Author contributions

I.V.F. designed and performed the experiments, built a fiber probe integrated with a microwave transmission line, analyzed the data, and prepared the graphic material. L.V.D.-A. contributed to experiments, performed calculations, analyzed the data, and prepared the graphic material. A.A.V. analyzed the performance of the microwave transmission line and contributed to data analysis and illustration preparation. A.O.L. have optimized the microwave source, provided diamond microcrystals, and contributed to the design of the microwave transmission line. S.A.Z., A.B.F., D.A.S.-B. participated in project planning and discussions of the results, V.L.V. contributed to the design of the experiments and overall project planning, A.M.Z. designed and oversaw the experiments, analyzed the data, and wrote the paper.

Additional information

Competing financial interests: The authors declare no competing financial interests.

How to cite this article: Fedotov, I.V. *et al.* Electron spin manipulation and readout through an optical fiber. *Sci. Rep.* **4**, 5362; DOI:10.1038/srep05362 (2014).